JOURNAL OF GEOPHYSICAL RESEARCH, VOL. 103, NO. D20, PAGES 26,115–26,125, OCTOBER 27, 1998

Laboratory study of closed and dynamic flux chambers: Experimental results and implications for field application

Fang Gao

Air Quality Management Section, Delaware Department of Natural Resources and Environmental Control, Dover

S. R. Yates

Physics and Pesticide Unit, U.S. Salinity Laboratory, U.S. Department of Agriculture, Riverside, California

Abstract. Flux chambers are useful and convenient tools for measuring gas emissions at soil and water surfaces in agricultural, ecological, environmental, and engineering studies. In this experiment, a closed chamber and a dynamic chamber were tested to study their general behavior and to identify factors affecting flux measurement. The experiment was designed and conducted on the basis of a previous study where the behavior of these flux chambers was simulated using mathematical models. Emission of a volatile solvent (CH_2Cl_2) from a constant source was measured at the surface of a soil layer by both closed and dynamic chambers. Measurements from the closed chamber tests show that the average flux calculated over a placement time ($t_t - t_0$) by a linear model is smaller than the initial flux at $t_0 = 0$ but greater than the temporal flux at $t_t - t_{t-1}$. The results from the dynamic chamber tests indicate that the steady-state flux may underestimate the actual flux when the chamber is operating at low airflow rates but overestimate the actual flux at high airflow rates. The underestimate at a low airflow rate is probably due to a depression on the diffusive flux at the enclosed soil surface, while the overestimate is due to a pressure deficit present within the chamber headspace that induces an advective flux from the covered soil matrix. The vacuum system operating the dynamic chamber in this experiment was found to be a predominant source of the pressure deficit. The air permeability of soil matrix and its surface condition are demonstrated to be important factors that determine how significant the effect of the pressure deficit is. In general, the experimental results agree with the simulation results reported previously. When using closed chambers, it is recommended that appropriate nonlinear models be used to calculate flux. When using dynamic chambers, which are more desirable, relatively high airflow rates should be employed and the pressure deficit within the chamber headspace should be measured and minimized.

1. Introduction

Enclosure-based methods, including passive (or closed) and active (or dynamic) flux chambers, have been widely used for measuring gas emissions at soil and water surface to the atmosphere [e.g., *Denmead*, 1979; *Sanders et al.*, 1985; *Balfour et al.*, 1987; *Gholson et al.*, 1991; *Yagi et al.*, 1995; *Czepiel et al.*, 1995; *Yates et al.*, 1996]. Various assumptions are applied to these chamber methods, and models based on these assumptions have been developed and used to calculate fluxes from the data obtained by these chambers [*Rolston*, 1986; *de Mello and Hines*, 1994; *Gao et al.*, 1997]. For example, a linear model has been used for closed chambers, assuming that the flux at the enclosed soil surface is relatively constant and uniform, a well-mixed condition is present within the chamber headspace, and the concentration within the chamber headspace increases linearly with time. For dynamic chambers, common assumptions include that the chamber is operating at a steady state, a well-mixed condition exists in the chamber, and a constant and uniform flux is present at the covered soil surface. Under these assumptions a simple model has been used for calculating the steady-state flux [*Rolston*, 1986; *Gao et al.*, 1997]. Because of their simplicity and ease in fabrication and operation the flux chambers and the associated flux models have been used extensively for measuring emissions of a variety of gases, including trace gases and volatile organic compounds (VOCs), although some of the assumptions associated with these methods may not be entirely valid under the real-world situations. Summary and comments on the advantages and disadvantages of these chamber methods can be found in the works of *Rolston* [1986], *Wesely et al.* [1989], and *Denmead and Raupach* [1993].

It is often cited that a closed chamber underestimates the actual flux due to mass accumulation or concentration buildup within the chamber headspace, while a dynamic chamber overestimates the actual flux due to a pressure deficit present inside the chamber caused by drawing an airstream through the chamber [*Rolston*, 1986; *Denmead and Raupach*, 1993]. The underestimate bias of closed chambers has been demonstrated in some experiments where the concentrations within the chamber headspace showed a nonlinear increase with time, or where the fluxes measured by closed chambers were compared with those measured by dynamic chambers [e.g., *Moore and Roulet*, 1991]. When applying closed chambers, most investi-

Paper number 98JD01346.
0148-0227/98/98JD-01346$09.00

gators limit chamber placement time to a short period in which the target gas concentration changes linearly with time, assuming a steady and uninhibited flux density at the covered soil surface [*Rolston*, 1986; *Wesely et al.*, 1989]. The overestimate of dynamic chambers due to the pressure deficit has also been shown in some previous studies [*Kanemasu et al.*, 1974; *Denmead and Raupach*, 1993]. For dynamic chambers, no studies have been reported on the effect of mass accumulation within chamber headspace on flux. This effect may be significant when the flow rate of airstream through a dynamic chamber is low, i.e., the resident time of the target chemical in the chamber is long. When reducing the resident time by increasing the airflow rate, the pressure deficit will usually increase, and so does its effect on the flux measurement. These issues have not yet been studied systematically.

In an earlier paper we developed mathematical models to simulate the general behavior of both closed and dynamic chambers [*Gao and Yates*, this issue]. The aim of the simulation study was to demonstrate how closed and dynamic chambers behave under various conditions and how different physical factors affect flux measurement performed by these chambers. The simulation results for closed chambers agree, in general, with the findings reported in the literature. The average flux measured by a closed chamber during its placement is shown to underestimate the actual flux. In addition, the simulation demonstrates that when the concentration of the target gas in the chamber headspace increases linearly with time, the average flux is still an underestimate because the linear increase in concentration is associated with a linearly decreasing flux at the covered surface, not a constant or uninhibited flux, as often assumed. The simulation results for dynamic chambers indicate that these chambers may produce an overestimate, as well as an underestimate, of the actual flux. When the chamber is operating at a low airflow rate and at surface of a soil with a low air permeability, the chamber is likely to underestimate the actual flux due to the presence of a relatively high concentration of the target gas within the chamber headspace. A dynamic chamber may overestimate the actual flux when the chamber is operating at a high airflow rate and at surfaces of soils with a high permeability due to the effect of the pressure deficit.

In this laboratory study we conducted a series of tests in which both closed and dynamic chambers were used to measure fluxes of a volatile compound (CH_2Cl_2) at soil surface. The experimental results, comparison of closed and dynamic chambers, comparison of the experimental results with the simulation results, as well as some implications of the experimental results for field application are presented and discussed.

2. Theoretical Basis

One assumption used in developing chamber behavior models is that the emission of a target gas from soil matrix into the atmosphere is a diffusive process which is driven by the concentration gradient across the soil-atmosphere interface [*Gao and Yates*, this issue]

$$J_g(t) = h[C_0^s(t) - C^a(t)] \tag{1}$$

where t (T) is time, $J_g(t)$ (M L^{-2} T^{-1}) is the flux density at the soil surface, $C_0^s(t)$ (M L^{-3}) is the target gas concentration at the soil-air interface on the soil side, $C^a(t)$ (M L^{-3}) is the target gas concentration above soil surface, and h (L T^{-1}) is the transport coefficient of the target gas through the soil-air interface. When a flux chamber is placed at soil surface, $C^a(t)$ is the space-averaged or well-mixed gas concentration in the chamber headspace. At $t = 0$, i.e., just before the chamber placement, $C_0^s(0) = C_0^s$ is assumed to be a constant and $C^a(0)$ is zero, and (1) becomes

$$J_g(0) = hC_0^s = J_0 \tag{2}$$

which is defined to be the actual flux being measured by a closed or dynamic flux chamber.

2.1. Closed Chamber

After a shallow closed chamber is placed at the soil surface, the concentration of the target gas in the chamber headspace, $C^a(t)$, and the flux density of the target gas at the enclosed soil surface, $J_g(t)$, can be written as [*Gao and Yates*, this issue]

$$C^a(t) = C_0^s\left[1 - \exp\left(-\frac{h}{V/A}t\right)\right] \tag{3}$$

$$J_g(t) = J_0\left[1 - \frac{C^a(t)}{C_0^s}\right] \tag{4}$$

where V (L^3) is the chamber volume, and A (L^2) is the soil surface area enclosed by the chamber. The V/A (L) ratio will be the chamber height or thickness (H), if the chamber has a uniform cross-section area equal to A. In practice, a linear model is often used to calculate an average flux density [*Matthias et al.*, 1980; *Rolston*, 1986]

$$\bar{J}_g = \frac{V}{A}\frac{\Delta C}{\Delta t} \tag{5}$$

where $\bar{J}_g$ (M L^{-2} T^{-1}) is the average flux density, and ΔC (M L^{-3}) is the concentration change measured in the chamber headspace in a short time span Δt.

2.2. Dynamic Chamber

We limit our discussion to the steady state of the chamber operation, because (1) operational experiences as well as our simulation results show that a dynamic chamber can reach a steady state within a short period of time after placement at a given airflow rate, and (2) flux measurements (i.e., gas samples) are taken almost always at the steady state in field applications of dynamic chambers. At steady state, the target gas concentration in the airstream, C_{steady} (M L^{-3}), and the flux density at the covered soil surface, J_{steady} (M L^{-2} T^{-1}), can be written as [*Gao and Yates*, this issue]

$$C_{\text{steady}} = C_0^s\frac{h}{Q/A + h}\left(1 + \frac{f_{\text{sair}}}{h}\right) \tag{6}$$

$$J_{\text{steady}} = J_0\left(1 - \frac{h}{Q/A + h}\right)\left(1 + \frac{f_{\text{sair}}}{h}\right) \tag{7}$$

where Q (L^3 T^{-1}) is the airflow rate, f_{sair} (L T^{-1}) is the volume air flux from the soil matrix into the chamber induced by a pressure deficit (ΔP) within the chamber headspace, and other terms are defined previously. The air flux (f_{sair}) can be expressed using an equation analogous to Darcy's equation [*Corey*, 1986; *Gao and Yates*, this issue]

$$f_{\text{sair}} = \frac{k_{sa}}{\mu_{sa}}\frac{\Delta P_Z}{Z} \tag{8}$$

where k_{sa} (L^2) is the air permeability of the soil matrix, μ_{sa} ($M\ L^{-1}\ T^{-1}$) is the viscosity of the soil air. If we define the pressure deficit (ΔP) to be the magnitude of pressure difference between the airstream within the chamber and the relatively stagnant air phase in the soil matrix, it can be estimated using Bernoulli's equation [*Vennard and Street*, 1975; *de Nevers*, 1991]

$$\Delta P = \tfrac{1}{2}\rho_{air}V_{air}^2 = \tfrac{1}{2}\rho_{air}\left(\frac{Q}{WH}\right)^2 \quad (9)$$

where ρ_{air} ($M\ L^{-3}$) is the density of the airstream through the chamber, V_{air} ($L\ T^{-1}$) is the velocity of the airstream through the dynamic chamber, and W (L) and H (L) are the chamber width and height, respectively, of the dynamic chamber used in this study. Equation (9) neglects the effect of air movement outside the chamber. This was approximately valid in our experiments since our preliminary tests showed that the air movement outside the chamber did not have a noticeable effect on pressure measurement. In addition to ΔP expressed in (9), a vacuum (or a blower) commonly used to operate the chamber system will also contribute to the pressure change inside the chamber. We will discuss this aspect later. If we combine (6) and (7), the following simple model can be obtained to calculate the steady-state flux [*Rolston*, 1986; *Gao et al.*, 1997]

$$J_{steady} = \frac{Q}{A}(C_{out} - C_{in}) \quad (10)$$

where C_{in} ($M\ L^{-3}$) and C_{out} ($M\ L^{-3}$) are the target gas concentrations measured in the chamber incoming airstream and outgoing airstream, respectively.

3. Materials and Methods

3.1. Experimental Setup

The experimental system used in this study is shown in Figure 1. During the experiment the system was placed under a laboratory fume hood at an ambient temperature of 25°C. A gas chromatograph (HP 5890 series II, Hewllett-Packard Co., Avondale, Pennsylvania), equipped with an electron capture detector (ECD) and supported by an automated sampler (Tekmer 700, Teckmer Co., Cincinnati, Ohio), was used for target gas analysis (the gas chromatograph and the automated sampler are not shown in Figure 1). The experimental system was designed to simulate a situation where an emission occurred from a constant vapor source at a certain depth below the soil surface. The components of the system and the experimental procedures are described in detail below.

3.2. Soil Matrix

The soil matrix was packed in an open-top box which had a width of 60 cm, a length of 60 cm, a depth of 30 cm, and was made of 20-gauge galvanized sheet metal. The thickness of the soil matrix was 20 cm, leaving a 10-cm footspace as a source compartment for the target gas (Figure 1). Two soils were used in the experiment: mixture of commercially available numbers 60 and 90 (ratio 1:2) fine sand, and number 12 coarse sand. The air permeabilities of these two media were estimated to be 3.2×10^{-6} and 3.0×10^{-5} cm^2, respectively, from their saturated hydraulic conductivities measured by the falling head method [*Klute and Dirksen*, 1986; *Massmann*, 1989]. Two upper boundary conditions were applied to the soil matrix: (1) open to the ambient air and (2) covered with one layer of high-density polyethylene tarp (thickness of 0.025 mm) commonly used in agricultural fumigation.

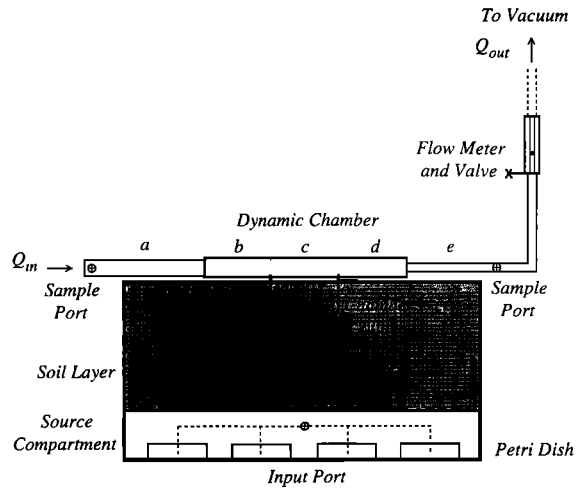

Figure 1. Experimental setup with the dynamic chamber at the surface of the soil matrix.

3.3. Closed Chamber

A closed (passive) chamber with a length (L) of 10 cm, a width (W) of 10 cm, and a height (H) of 15 cm, fabricated with 22-gauge galvanized sheet metal, was used in the experiment. The inside surface of the chamber was sprayed with TFE (trifluoroethane) dry film lubricant (Fisher Scientific Co., Fair Lawn, New Jersey). A sample port was installed on one sidewall of the chamber. The gas samples were taken from the headspace of the chamber using an airtight glass hypodermic syringe. The sample port was sealed with a copper nail during a test except when gas samples were taken. A stainless steel tube, with an ID of 0.5 cm and length of 9 cm, was connected to the sample port and hung horizontally about 7.5 cm above the soil surface inside the chamber. Eight small holes were made on this sample tube. The holes were open to different directions so that the target gas could enter the sample tube from different directions at various locations along the tube during sampling. A manually operated fan was installed in the chamber. The fan has two blades made of fine stainless steel screen and fixed on a horizontal axis parallel to the sampling tube. Each blade has a dimension of 1 cm × 8 cm. In the experiment this fan was manually turned for 10 times to help mixing ~10 s prior to sampling. When operating at an open soil surface, the chamber was sitting on a base frame which had a collar into the soil matrix to a depth of 5 cm. The base frame was made of 24-gauge galvanized sheet metal attached to 0.6-cm (1/4 in.) angle aluminum. When used at the covered soil surface, the chamber was placed directly on the tarp and supported by the soil matrix below (the passive chamber is not shown in Figure 1).

3.4. Dynamic Chamber

The structural details and aerodynamic features of the dynamic chamber used in this experiment have been reported previously [*Gao et al.*, 1997]. The dynamic chamber used in this experiment had a width (W) of 20 cm, a length (L) of 19.8 cm, and a height (H) of 5 cm. A schematic diagram of this chamber is shown in Figure 1. In brief, the chamber has an inlet (a), an

Table 1. Test Identifications and Experimental Conditions

Test ID	Chamber Used	Soil Matrix	Soil Surface Condition
C-1	closed	fine sands	open
C-2	closed	fine sands	covered
C-3	closed	coarse sands	open
C-4	closed	coarse sands	covered
D-1	dynamic	fine sands	open
D-2	dynamic	fine sands	covered
D-3	dynamic	coarse sands	open
D-4	dynamic	coarse sands	covered

inlet transition zone (*b*), a main body (*c*) that covers the soil surface, an outlet transition zone (*d*), and an outlet (*e*). Within each transition zone, five separation baffles are installed to divide the zone into six individual channels to direct the airstream uniformly across the entire enclosed soil surface. In all channels of both transition zones, tangled fine copper wires were placed to help mixing. Aerodynamic tests in the laboratory have shown that the special structure of this chamber can create a relatively uniform airstream in the chamber main body at a given airflow rate [*Gao et al.*, 1997]. The airstream through the chamber was created by a laboratory vacuum at the chamber outlet side. The flow rate of the airstream was regulated by a valve and monitored by a Manostat ball flowmeter (Manostat Corp., New York).

3.5. Chemical Vapor Source

Methylene chloride (CH_2Cl_2), a volatile solvent commonly used in industry, was used in this experiment. This chemical has a boiling point of 40°C, and evaporation from its liquid phase under ambient temperature (25°C) can provide a vapor source of constant concentration. In this experiment, CH_2Cl_2 liquid, with a purity ≥99.9% (Fisher Scientific Co., Fair Lawn, New Jersey), was first introduced through the input port into four glass petri dishes sitting at the bottom of the source compartment (Figure 1). The chemical liquid was allowed to evaporate from the petri dishes for about 8 hours to establish a steady emission at the soil surface before a chamber was placed at the soil surface to measure the emission rate (i.e., flux density). The air under the fume hood was continuously purged and vented to the outside during the entire experiment.

3.6. Closed Chamber Tests

Four tests were conducted with the closed chamber. Conditions of these tests are listed in Table 1. The chamber placement times in the tests ranged from 55 to 90 min, which were longer than the placement time of less than 30 min commonly reported in the literature. The reason for using longer placement times was to observe how the shallow closed chamber behaved in extended placement periods. Two replicated runs were conducted for tests C-1 and C-3 and four runs for tests C-2 and C-4 ("C" for "closed chamber"). During each individual run, a 2-mL gas sample (~0.1% of the chamber headspace volume) was taken every 3, 5, 6, or 10 min from the chamber headspace with a glass hypodermic syringe. The gas sample was transferred into a 21.6-mL glass vial, which was sealed with a Teflon-lined cap immediately after the sample transfer. The concentration of the target gas (CH_2Cl_2) in each sample vial was determined by the GC-Sampler system. When an individual run was finished, the chamber was removed and its interior was flushed by clean air. In the tests on the covered surface (tests C-2 and C-4), gas samples were also taken during each individual run from underneath the tarp to determine the target gas concentration immediately under the tarp.

3.7. Dynamic Chamber Tests

Four similar tests were conducted with the dynamic chamber, D-1, D-2, D-3, and D-4 ("D" for "dynamic chamber"), as indicated in Table 1. In each test, the chamber was operated at steady state at different airflow rates, from 3 to 132 L min^{-1}. The chemical residence times with respect to these airflow rates are estimated to be from 40 to 1 s, correspondingly. At each flow rate, the chamber was first allowed to operate for 20 to 30 min to reach a steady state. Three replicate gas samples were then taken at the chamber inlet and outlet to determine CH_2Cl_2 concentrations in the incoming airstream and the outgoing airstream, using the same procedures in the passive chamber tests. In a preliminary experiment we found that the dynamic chamber used in this experiment could reach a steady state at various airflow rates in 5–15 min. To further verify this, gas concentration in the incoming and outgoing airstreams in the transient stage of test D-1 were monitored for 20 min at three different flow rates (6, 61, and 130 L min^{-1}). These three flow rates cover the entire range of the flow rates used in this experiment. Again, the target gas concentration immediately under the tarp was measured in the two tests on the covered soil surfaces (tests D-2 and D-4). For all four tests with the dynamic chamber the pressure deficits within the chamber, with respect to the ambient pressure, were measured at different airflow rates with a low-range pressure transducer (0–25 Pa, model PX653-0.1D5V, Omega Engineering, Inc., Stamford, Connecticut) and a digital data logger for data acquisition (micrologger model 21X, Campbell Scientific, Inc., Logan, Utah).

4. Results and Discussion

4.1. Closed Chamber Tests

4.1.1. Concentration in chamber headspace. Figure 2 shows the target gas concentrations measured in the chamber headspace from two closed chamber tests on the fine sand. The concentration data obtained from two separate runs in test C-1 (at open surface) show a linear increase at early time but a nonlinear or exponential increase when the chamber placement time was extended (Figure 2a). The data from four separate runs in test C-2 (at covered surface) show basically a linear increase, except that a slight exponential trend exists toward the end of the extended placement in run 4 (Figure 2b). The difference in the concentration increase between test C-1 and test C-2 is likely due to the absence or presence of the polyethylene tarp at the soil surface. In test C-2 the tarp at the soil surface presented an actual physical barrier for the chemical transport. This physical barrier increased significantly the interfacial resistance and thus reducing the magnitude of the transport coefficient (h), for the gas transport through the soil-air interface. For a given timescale the effect of a reduced h is to attenuate the exponential increase of the target gas concentration in the chamber headspace.

Figure 3 shows the concentration data obtained in tests C-3 (at open surface of the coarse sand) and C-4 (at covered surface of the coarse sand). The concentration curves in Figures 3a and 3b show trends similar to those in Figures 2a and 2b, and thus similar discussion and explanations apply. The difference in magnitude of concentrations in runs 1 and 2 of

test C-3 (Figure 3a) was due to the exhaustion of CH_2Cl_2 liquid in the source compartment, which was detected during the test. In this test, run 2 was conducted ~35 min after run 1, thus a lower emission was measured at the soil surface. If we compare Figures 3 with 2, we can see that the rates of concentration increase in test C-3 and C-4 seem lower than those observed in tests C-1 and C-2. The more rapid rates of concentration increase from the fine sand tests (C-1 and C-2) are likely due to higher source concentrations. In tests C-1 and C-2 the target gas concentrations in the source compartment were 1777.8 and 1929.3 mg/L, respectively, while in tests C-3 and C-4, the source concentrations were 1480.8 and 1790.7 mg/L, respectively (the concentrations are averaged values of six samples measured during individual tests).

4.1.2. Flux density calculations. The concentration data obtained from the passive chamber tests are used to calculate flux densities at the soil surface. Since two different upper boundary conditions were used in these tests, flux calculations are slightly different for different tests, as described and discussed below.

We use (5) to calculate flux for the tests at the open surfaces of the fine sands (test C-1) and the coarse sands (test C-3). In the calculation, $\Delta C = C_i - C_0$ is used to calculate an average flux in a time span of $\Delta t = t_i - t_0$, while $\Delta C = C_i - C_{i-1}$ is used to calculate a temporal flux in a short time span of $\Delta t = t_i - t_{i-1}$. The subscript i specifies the ith sample taken at time t_i, and C_0 is assumed to be zero at $t_0 = 0$. The results of the calculation are shown in Figure 4, in which the solid curves are results of the average fluxes, while the dashed curves are the temporal fluxes. Figure 4 indicates that the average flux decreases as the chamber placement time (t_i) increases. This implies that $\bar{J}_i$ during $t_i - t_0$ is an underestimate of the flux density at $t_0 = 0$, and the degree of underestimate becomes more severe as the chamber placement time is extended. The temporal flux curves in Figure 4 show that (1) the degree of their underestimate is more severe than the average fluxes at most of the time points, especially when the placement time was extended and (2) the temporal flux values are fluctuating while decreasing with time.

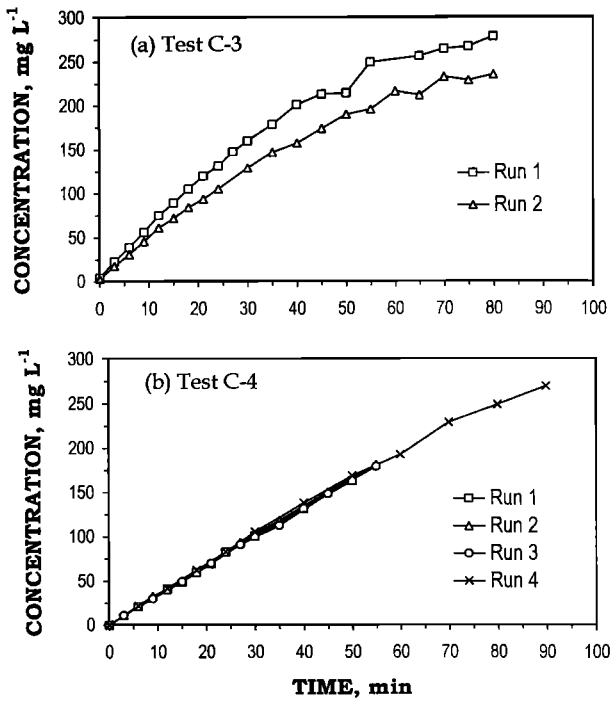

Figure 3. Concentration of CH_2Cl_2 inside the closed chamber measured in the tests with coarse sand. (a) Test C-3 at the open surface, (b) test C-4 at the covered surface.

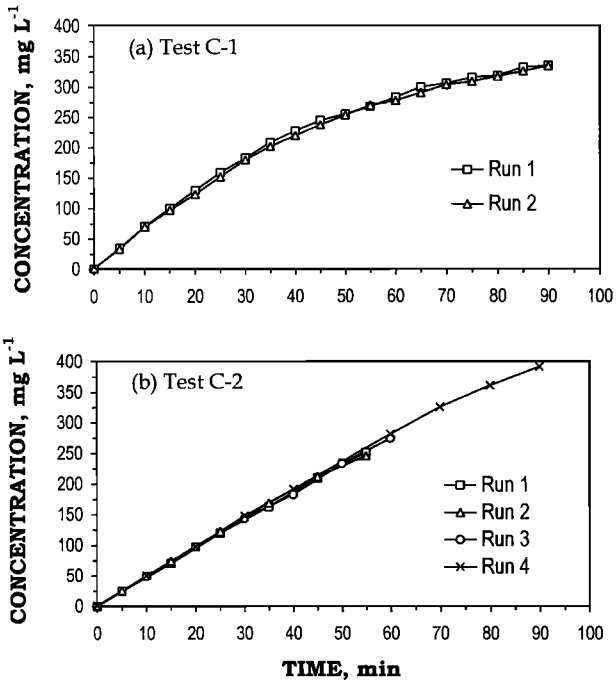

Figure 2. Concentration of CH_2Cl_2 inside the closed chamber measured in the tests with fine sand. (a) Test C-1 at the open surface, (b) test C-2 at the covered surface.

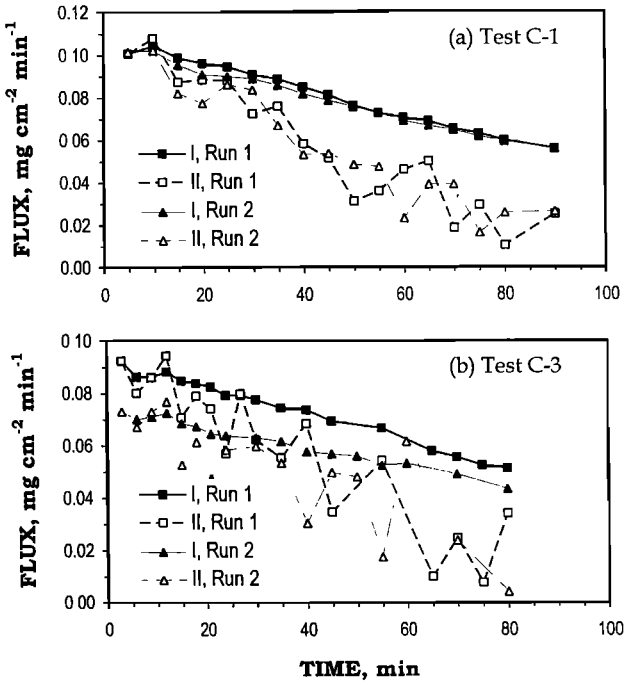

Figure 4. Flux densities calculated for the closed chamber tests at the open soil surface of (a) fine sand and (b) coarse sand. I, average fluxes; II, temporal fluxes.

Table 2. Estimated h and J_0 for Closed Chamber Tests at Covered Soil Surfaces

Test	Concentration Under Tarp,[a] mg L^{-1}	Estimated h, cm s^{-1}		Calculated J_0, mg cm^{-2} min^{-1}	
		Average	Range	Average	Range
C-2	1394.5	0.00091	0.00086–0.00095	0.076	0.072–0.079
C-4	1158.6	0.00076	0.00072–0.00079	0.053	0.050–0.055

[a] Average concentration of six samples measured during each test.

For the tests at the covered surfaces of the fine sand (test C-2) and the coarse sand (test C-4) the average and temporal fluxes are also calculated using (5). In addition, (3) is used to estimate the interfacial transport coefficient (h_t), using the concentration measured under the tarp (as C_0^s) and the concentration in the chamber headspace $C^a(t_t)$ at time t_t. The estimated h_t is then used to calculate J_0 in (2). The results of the calculation are summarized in Table 2. The average values in Table 2 are calculated from 26 values in test C-2 and 34 values in test C-4. The fluxes calculated from different methods are plotted in Figure 5. We include only runs 1 and 4 of tests C-2 and C-4 in Figure 5, since the calculation results for all other runs have the similar trends. From Figure 5 it can be seen that the average flux decreases with the chamber placement time, and the temporal flux decreases with time as well but in a faster and fluctuating manner. The transport coefficient (h) has a relatively constant value as estimated by (3) and so does the initial flux (J_0) as estimated by (2). The temporal flux $J_g(t_t)$, as estimated by (4), is also plotted in Figure 5. It should be noted from all four figures in Figure 5 that the average flux densities (solid square) fall between the estimated initial flux J_0 (solid triangle) and the temporal flux $J_g(t_t)$ (open triangle).

5. Dynamic Chamber Tests

5.1. Transient Stage of Test D-1

Concentrations of the target gas (CH_2Cl_2) in the chamber airstream in three transient stages of test D-1 are plotted as a function of time in Figure 6 (precisely, the concentration data in Figure 6 are the target gas concentrations in the outgoing airstream minus the concentrations in the incoming airstream). It can be seen clearly that the dynamic chamber reached a steady state at each of the three flow rates in a short period of time after the chamber placement. Comparison of these curves indicates that the greater the airflow rate, the faster the chamber reaches the steady state. It was also observed that the concentration of the target gas at the steady state is not simply proportional to the flow rate. Since the chamber was operating in the same emission event, the nonlinear relation implies that the chamber was producing different flux values at different airflow rates. This issue will be further discussed later.

5.2. Steady State Tests at Open Soil Surfaces

Figure 7a shows the measured steady-state concentrations ($C_{steady} = C_{out} - C_{in}$) and the flux densities calculated by (10) as a function of airflow rates (Q) and Q/A ratios. From Figure 7a it can be seen that when the airflow rate is in the lower range (e.g., Q less than about 20 L min^{-1}), the steady-state concentration of the target gas (C_{steady}) decreases rapidly

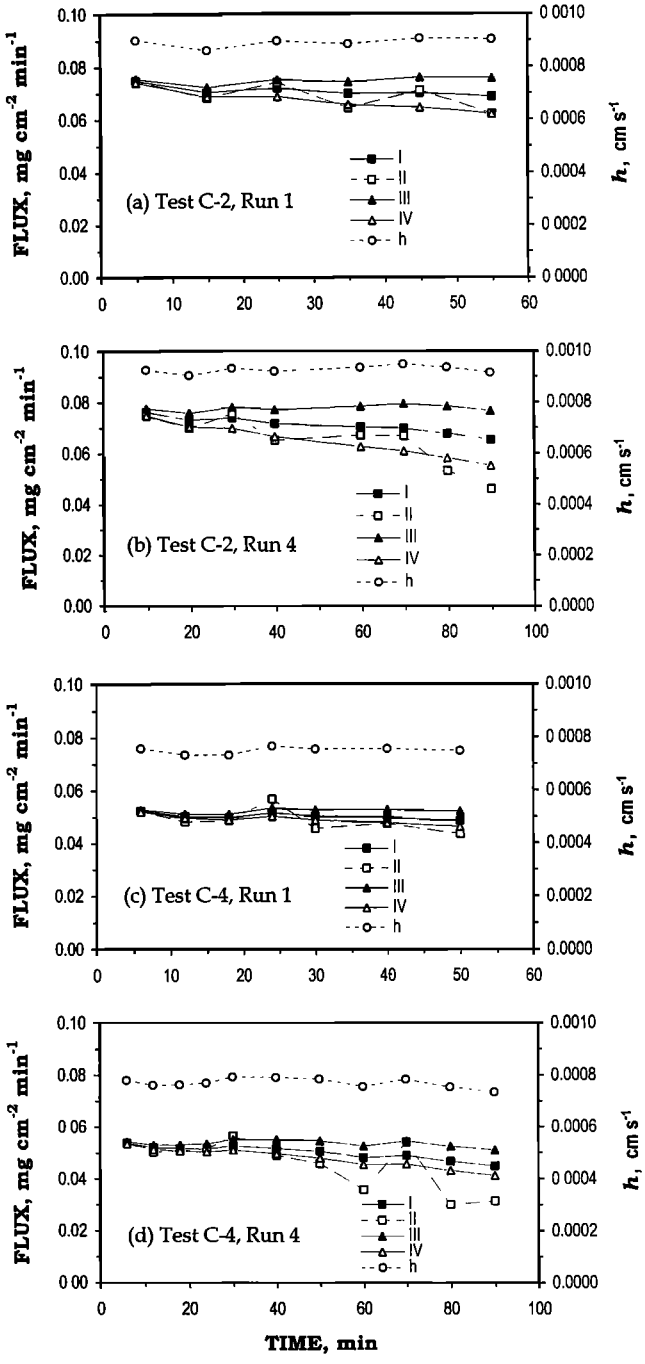

Figure 5. Flux densities calculated for the closed chamber tests at the covered soil surface (a and b) of fine sand, and (c and d) coarse sand. I, average fluxes; II, temporal fluxes; III, from equation (2); IV, from equation (4); and h, from equation (3).

as Q increases. In the same range, the steady state flux (J_{steady}) increases rapidly. When the flow rate increases beyond this range, the rapid decrease of the steady-state concentration becomes a gradual decrease, and the rapid increase of steady-state flux turns to a gradual increase. The changing trends of both C_{steady} and J_{steady} follow closely the patterns obtained in our simulation study [*Gao and Yates*, this issue].

Figure 7b shows the pressure deficit measured during test D-1 (ΔP_m, where the subscript m stands for measured). The initial reason that we measured the pressure deficit was to assess whether (9) could be adequate for estimating the pressure deficit and how the pressure deficit would affect the fluxes being measured. From (9) the maximum pressure deficit within the range of the flow rates used in the experiment is 0.03 Pa. However, the actual maximum pressure deficit measured during the test was 1.80 Pa, about 2 orders of magnitude greater than the estimated value. The comparison indicates that when a vacuum system is used to draw air through a dynamic chamber, it contributes significantly to the pressure deficit within the chamber.

The dashed curve in Figure 7a is plotted using (7) to describe the steady-state behavior of the dynamic chamber as a function of airflow rate. To calculate f_{sair}, (8) was used with the measured k_{sa} of 3.2×10^{-6} cm^2, a μ_{sa} of 0.18 mg cm^{-1} s^{-1} [*Massmann*, 1989], a Z of 20 cm (depth from soil surface to source compartment), and the measured pressure deficits shown in Figure 7b. To estimate the transport coefficient (h), we adopted the following model proposed by *Jury et al.* [1983]:

$$h = \frac{D^a}{d} \tag{11}$$

where D^a is the diffusion coefficient of the target gas in air, and d is the thickness of a stagnant air layer at the soil surface. The diffusion coefficient of CH_2Cl_2 in air at 25°C, as estimated by the Fuller-Schettler-Giddings method [*Reid et al.*, 1987], is 0.105 cm^2 s^{-1}. Although the value of d is likely to vary depending on the strength of air movement and mixing above the soil surface, *Jury et al.* [1983] and *Simunek and van Genuchten* [1994] show that a d value of 0.5 cm is a good average of a bare soil surface. We will discuss the effect of airstream in the chamber on the stagnant air layer later. Using the above D^a and d, we obtained an h value of 0.21 cm s^{-1}. With an estimated J_0 of 0.50 mg cm^{-2} min^{-1} the dashed curve in Figure 7a shows that the simulation by (7) can describe closely the measured fluxes in test D-1.

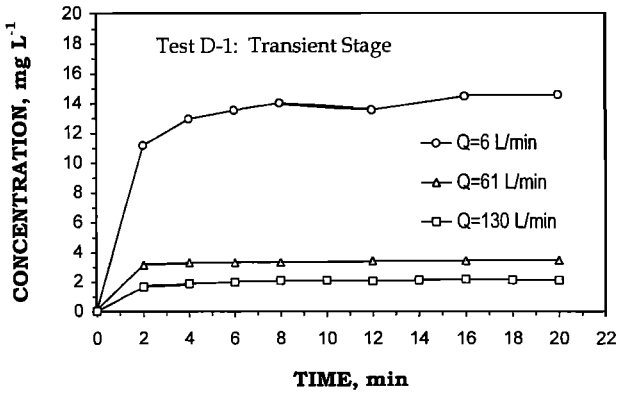

Figure 6. Transient stage of the dynamic chamber test D-1 at the open surface of fine sand.

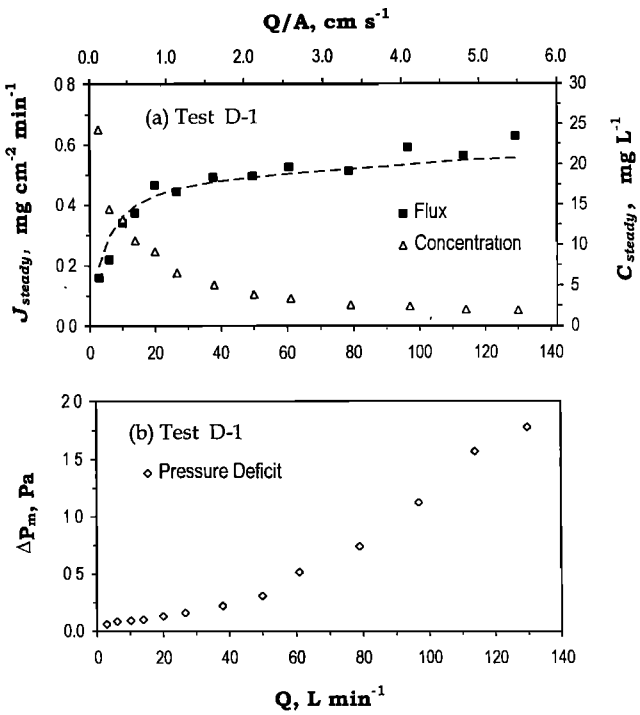

Figure 7. Steady-state concentrations and calculated flux densities for the dynamic chamber test D-1 at the open surface of fine sand. (a) Measured concentrations ($C_{steady} = C_{out} - C_{in}$) and flux densities calculated by equation (6), (b) measured pressure deficit (ΔP_m).

The experimental data from test D-3 are plotted in Figure 8 and show the steady-state concentration of the target gas ($C_{steady} = C_{out} - C_{in}$) and the flux calculated by (10) (Figure 8a) and the pressure deficit measured during the test (ΔP_m) (Figure 8b). A similar discussion and explanations apply to Figure 8. It should be noted that the effect of the pressure deficit on the flux is more profound, especially when the airflow rate is high. If we compare Figures 7 with 8, we can see that at high airflow rates the effect of the pressure deficits on the measured fluxes is significantly greater at the open surface of the coarse sands than at the open surface of the fine sands. This is likely due to the higher permeability of the coarse sands, since the pressure deficit at a high airflow rate may induce a significant advective mass flow out from the coarse sand matrix. The comparison indicates that the permeability of the soil matrix has a significant effect on the behavior of the dynamic chamber at high airflow rates. This is in agreement with our simulation results [*Gao and Yates*, this issue].

The dashed curve in Figure 8a shows the simulation of steady-state flux of test D-3 using (7) under the experimental condition. The measured k_{sa} of 3.0×10^{-5} cm^2 for the coarse sand, an estimated J_0 of 1.30 mg cm^{-2} min^{-1}, and the measured pressure deficits (Figure 8b) were used in the simulation. The simulated curve shows that (7) can describe reasonably well the measured fluxes in test D-3.

5.3. Steady State Tests at Covered Soil Surfaces

Similarly, we plot the experimental data of test D-2 in Figure 9, where Figure 9a shows the steady-state concentration ($C_{steady} = C_{out} - C_{in}$) and the flux density calculated by (10) as a function of airflow rates and Q/A ratios, and Figure 9b

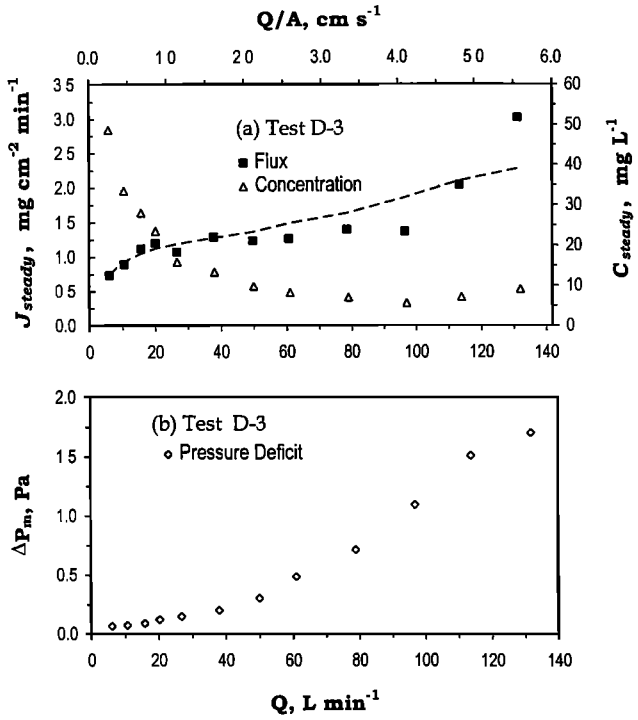

Figure 8. Steady-state concentrations and calculated flux densities for the dynamic chamber test D-3 at the open surface of coarse sand. (a) Measured concentrations ($C_{steady} = C_{out} - C_{in}$) and flux densities calculated by equation (6), (b) measured pressure deficits (ΔP_m).

shows the pressure deficit (ΔP_m) measured during the test. Since we measured the target gas concentration below the tarp, which can be used as C_0^s, we can use (6) to estimate the interfacial transport coefficient (h), assuming f_{sair} is zero. The results are also plotted in Figure 9b.

The flux densities in Figure 9a show a rapid increase at low airflow rates but remain at a relatively steady value as the airflow rate further increases. At low airflow rates, multiple factors may contribute to the control of the target gas emission at the soil surface. The plastic tarp is obviously a factor since it physically hinders the transport of the target gas through the soil-air interface. Changes in concentration gradient across the soil-air interface is a factor. The steady-state concentration within the chamber headspace decreased drastically with the airflow rate in this lower range, but the concentration under the tarp remained constant during the test. The stagnant air layer over the tarp is also a contributing factor. As the airflow rate increases, the thickness of this stagnant air layer is likely to approach its minimum quickly, and so is its resistance to the gas transport. When the airflow rate further increases to over 40 L min^{-1}, the resistance of the plastic tarp becomes dominant in controlling the gas transport and thus the emission. Although the pressure deficit increases significantly with airflow rate in the higher range (Figure 9b), the tarp acts as a physical barrier to the advective gas transport. At high airflow rates, the concentration gradient across the tarp did not change significantly with a steady-state concentration near zero in the chamber headspace.

Figure 9b shows that the transport coefficient (h) increases with Q but becomes relatively constant when Q exceeds 20 L min^{-1}. This indicates that at high airflow rates the transport coefficient is determined mainly by the resistant nature of the plastic tarp at the soil surface. The tarp-dominated h in test D-2 is approximately 0.0017 cm s^{-1} (Figure 9b). This value falls well into the range estimated for the same tarp in a field experiment by *Wang et al.* [1997]. With the estimated h values in Figure 9b and the measured C_0^s of 1264.36 mg L^{-1}, we can use (2) and (7) to simulate the steady-state flux as a function of the airflow rate. The result is shown by the dashed curve in Figure 9a. In the calculation, we neglect f_{sair} in (7) because of the presence of the high-density polyethylene tarp at the soil surface. The simulation shows again that the measured fluxes can be described well by (7).

The experimental data from test D-4 are plotted in Figure 10 to show the steady-state concentration ($C_{steady} = C_{out} - C_{in}$) and the flux density calculated by (10) (Figure 10a) and the pressure deficit measured during the test (ΔP_m) and the values of h estimated using (6) (Figure 10b). A discussion and explanations similar to those for Figure 9 apply to Figure 10. It should be noted that the behavior of the dynamic chamber is essentially the same in tests D-2 and D-4. This indicates that surface conditions in these two tests control the emission of the target gas. Because of the presence of the plastic tarp at the surface, the permeability of the soil matrix under the tarp seems to play a minor role, and the pressure deficit seems to have an insignificant effect on the emission at the covered soil surface. The behavior of the dynamic chamber at the covered

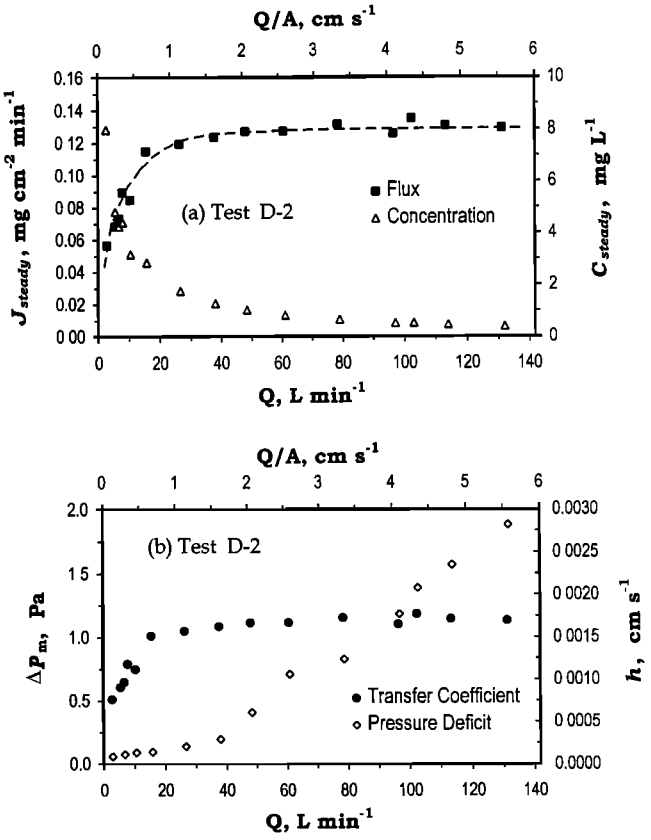

Figure 9. Steady-state concentrations and calculated flux densities for the dynamic chamber test D-2 at the covered surface of fine sand. (a) Measured concentrations ($C_{steady} = C_{out} - C_{in}$) and flux densities calculated by equation (6), (b) measured pressure deficits (ΔP_m) and estimated transfer coefficient (h).

soil surface is similar to the simulated patterns at the surface of soils with low permeability or without the effect of pressure deficit, i.e., approaching a constant value as the airflow rate increases [*Gao and Yates*, this issue]. The dashed curve in Figure 10a is the steady-state flux simulated by (7), with the measured C_0' of 1256.69 mg L^{-1} and the estimated h values in Figure 10b. Again, the term f_{sair} in (7) was neglected in the calculation.

5.4. Comparison of Flux Densities Measured by Two Chambers

Flux densities obtained from both closed and dynamic chambers in this experiment are summarized in Table 3. For the closed chamber tests at open soil surfaces, a linear extrapolation in Figure 4 is used to obtain estimates of the flux densities at $t = 0$. Our simulation study shows that a linear extrapolation can give a close estimate of the flux at $t = 0$ [*Gao and Yates*, this issue]. For the closed chamber tests at covered soil surfaces, we adopt the estimated averages listed in Table 2. For the four dynamic chamber tests, the ranges of flux densities listed in Table 3 are from the lowest flux at the lowest airflow rate to the relatively stable flux in the range of 20–60 L min^{-1} (Figures 7a–10a).

At the covered soil surfaces, the flux densities measured by the dynamic chamber at the lowest airflow rate (3 L min^{-1} in this experiment) are very close to those measured by the closed chamber (0.06 versus 0.076 for the fine sand and 0.06 versus 0.053 for the coarse sand, Table 3). As the airflow rate increases to over 20 L min^{-1}, the fluxes from the dynamic chamber reach a stable value that is approximately twice as big as the fluxes measured by the closed chamber (0.13 versus 0.076 for the fine sand and 0.13 versus 0.053 for the coarse sand, Table 3). The flux of 0.13 mg cm^{-2} min^{-1} is the maximum flux that occurred under the given experimental conditions. On the other hand, we can reasonably expect from the experimental data that a flux smaller than 0.06 (mg cm^{-2} min^{-1}) would be obtained if the dynamic chamber was operated with an airflow rate smaller than 3 L min^{-1}.

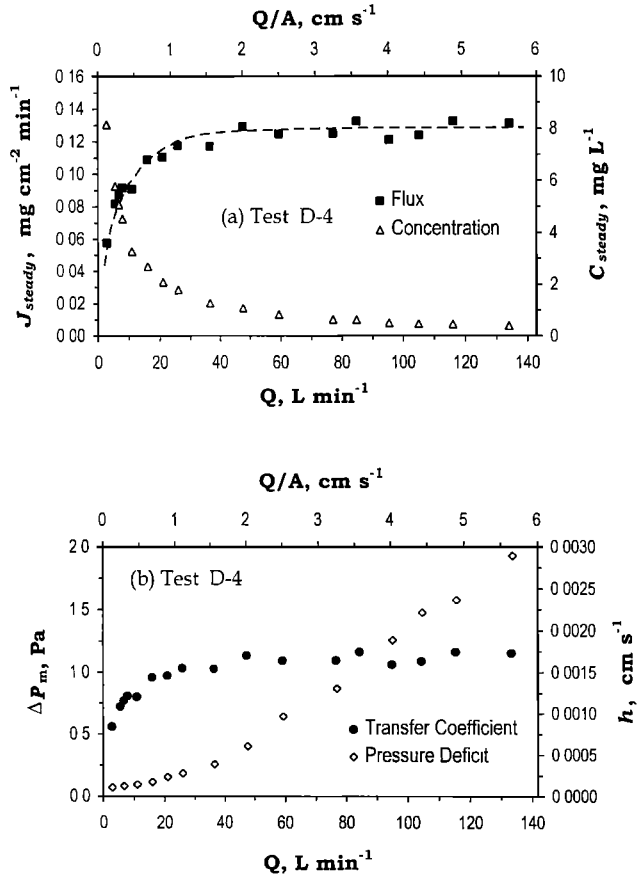

Figure 10. Steady-state concentrations and calculated flux densities for the dynamic chamber test D-4 at the covered surface of coarse sand. (a) Measured concentration ($C_{steady} = C_{out} - C_{in}$) and flux densities calculated by equation (6), (b) measured pressure deficits (ΔP_m), and estimated transfer coefficient (h).

Table 3. Flux Densities (mg cm^{-2} min^{-1}) Measured by Two Chambers

	Open Surface		Covered Surface	
Chamber	Fine Sand	Coarse Sand	Fine Sand	Coarse Sand
Closed	0.110[a]	0.095[a]	0.076[b]	0.053[b]
Dynamic	0.16–0.50[c]	0.70–1.30[c]	0.06–0.13[c]	0.06–0.13[c]

[a] Extrapolated in Figures 4 (a) and (b).
[b] Obtained from Table 2.
[c] Estimated from Figures 7a, 8a, 9a, and 10a.

At the open surface of fine sand, the flux density measured by the dynamic chamber at the lowest airflow rate is slightly greater than that measured by the closed chamber (0.16 versus 0.11, Table 3). The relatively stable value for the dynamic chamber, however, is about 5 times greater than the flux of the closed chamber (0.50 versus 0.11, Table 3). At the open surface of coarse sand, the flux from the dynamic chamber at the lowest airflow rate is about 7 times greater than that of the closed chamber (0.70 versus 0.095, Table 3), while the relatively stable value of the dynamic chamber is about 14 times greater than that of the closed chamber (1.30 versus 0.095, Table 3). This shows clearly that the air conductivity of the soil matrix has a significant impact on flux measurement of the dynamic chamber at the open soil surface. Such an impact is not shown on the fluxes measured by the closed chamber. In their recent study, *Bekku et al.* [1997] compared fluxes measured by their closed chamber and dynamic chamber. Their results are supportive to ours both qualitatively and quantitatively.

5.5. Pressure Deficit Within Dynamic Chamber

Measurements of the pressure difference between the airstream in the dynamic chamber and the ambient air show a deficit range from 0.1 to 2.0 Pa when the chamber airflow rate increases from 3 to 132 L min^{-1} (Figures 7b–10b). If we use (9) to estimate the pressure difference caused by the flowing air alone, we obtain a deficit range from 1.5×10^{-5} to 3.1×10^{-2} Pa, which is 4–2 orders of magnitudes smaller than the measured pressure deficit. Using Poiseuille's law to calculate the pressure difference across the inlet pipe gives a maximum value of 0.14 Pa, about 1 order of magnitude smaller than the measured maximum value. The comparison leads us to conclude that the vacuum system used to operate the dynamic chamber in this experiment is the dominant source of the pressure deficit. In practice, different dynamic chambers may

be operated by different mechanisms (e.g., vacuum, pump, or blower), and the actual response of the internal pressure to different chamber structures and operating systems may vary. For example, our recent tests show that the cross section and length of the chamber inlet pipe have a significant effect on the magnitude of the pressure deficit within the vacuum-operated chamber used in this experiment [*Gao and Yates*, 1997]. However, the pattern of the pressure response to the operating vacuum may be similar; that is, the pressure deficit increases as the airflow rate increases. This general pattern may be expected for other dynamic chambers operated by a vacuum from outlet.

5.6. Factors Affecting Flux Measured by Dynamic Chamber

All four tests with the dynamic chamber show clearly that the measured steady-state flux is a function of the chamber airflow rate. The change in airflow rate will change some physical factors in the chamber system, such as the concentration gradient across the soil-air interface, the resistance of the interface to the target gas transport, and pressure deficit within the chamber. Thus the effect of the airflow on the flux at the enclosed soil surface is a combination of effects of those factors.

The concentration of the target gas (CH_2Cl_2) in the chamber headspace decreases by ~4 times in all four tests when the airflow rate increases from 3 to 30 L min^{-1} (Figures 7a, 8a, 9a, and 10a). This rapid decrease of the headspace concentration implies an increase of the concentration gradient across the enclosed soil-air interface, assuming the target gas concentration in the soil matrix remains relatively constant (this is true for tests D-2 and D-4). From (1) it can be seen that the increase of the concentration gradient will enhance the diffusive flux. The interfacial resistance is likely to decrease as the airflow rate increases due to the reduction of the thickness of the stagnant air layer. The increase in pressure deficit with airflow rate also contributes to an increasing flux. Thus in the lower range of airflow rate, all these factors contribute to the overall effect on the surface flux. When the airflow rate increases over 30 or 40 L min^{-1}, the effect is likely dominated by the interfacial resistance for the tests at the covered soil surface and by the pressure deficit for the tests at the open soil surface.

The effect of the pressure deficit on the measured flux at the open soil surfaces observed in this experiment has a significant implication for chamber application in the field. When a dynamic chamber is used on permeable soils, care must be taken to control the magnitude of pressure deficit inside the chamber to limit the magnitude of overestimates. When operating on less permeable media, the overestimate will not be so much of a problem. However, overestimates may still occur when the pressure deficit becomes greater than a few tenths of a Pascal, as indicated in Figures 9 and 10.

A dynamic chamber may underestimate the actual flux when the airflow rate is very low. This is mainly due to the presence of a headspace concentration that is much higher than that above the soil surface outside the chamber (or before the chamber placement). As a result, the concentration gradient across the enclosed soil surface becomes smaller (or depressed) and thus driving a smaller diffusive flux. One possible solution to this problem is to select the airflow rate so that the steady-state concentration is close to that in the ambient air. *Bekku et al.* [1997] show in their recent study that when the headspace concentrations in dynamic chambers are close to the ambient concentrations, relatively accurate flux estimates can be obtained. An ideal situation is that a pressure deficit is present inside the chamber to induce a convective flux to compensate the depressed diffusive flux, so that an unbiased flux can be measured. The difficulties for obtaining this ideal situation are (1) the actual flux at the uncovered soil surface remains unknown and (2) a proper combination of airflow rate and pressure deficit is difficult to select, because the response between airflow rate and pressure deficit may by different in different dynamic chamber systems. If we use Q/A ratio as a general index for a dynamic chamber system, our experimental results suggest that the pressure deficit should be limited to a few tenths of a Pascal and a Q/A ratio to a range of 0.1–0.3 cm s^{-1}.

6. Concluding Remarks

From the experimental results and the discussion presented above, the following concluding remarks can be drawn.

1. The general behavior of both closed and dynamic chambers follows the results shown in our simulation study. Thus the models described in the previous paper can be used to predict the general behavior of both closed and dynamic chambers and the possible effect of various physical factors on the flux measurements performed by these chambers.

2. A closed chamber will lead to the underestimate of the actual flux density when a linear model is used to calculate an average flux. This underestimate is due to the decreasing nature of the flux density at the soil surface after chamber placement. This finding agrees with and provides additional explanation to the results reported by other chamber users. The longer the chamber placement time, the more severe the underestimate is.

3. A dynamic chamber may also underestimate the actual flux when the flow rate of the airstream is low. At a low airflow rate, the target gas concentration within the chamber headspace will build up to a magnitude high enough to depress the concentration gradient across the soil-air interface, even though clean air is flowing though the chamber continuously. Under such conditions the pressure deficit caused by the slow airstream and the operating vacuum may be too small to induce an advective flux significant enough to affect the total flux measured by the chamber.

4. A dynamic chamber will overestimate the actual flux when the airflow rates are high. This is especially true when the chamber is operating at the open surface of permeable medium, such as the coarse sands tested in this experiment. In a vacuum-operated chamber system the overestimate is probably due to the effect of pressure deficit, which is caused by the operating vacuum rather than the flowing airstream. For blower-operated chamber systems, additional studies are needed to assess the pressure change inside the chambers and the effect of such pressure change on flux measurement.

5. To minimize the bias of underestimate or overestimate, a dynamic chamber should be operated under an ideal situation where the diffusive flux depressed by the concentration buildup can be compensated by a convective flux induced by the pressure deficit. The ideal combination of airflow rate and pressure deficit is probably case specific and difficult to assess. For vacuum-driven chamber systems, it is suggested that relatively high airflow rates be employed while the pressure deficit in the chamber headspace be measured and minimized.

Acknowledgments. The authors thank J. Gan and Q. Zhang for their help in obtaining experimental data presented in this paper.

References

Balfour, W. D., C. E. Schemata, and B. M. Elkhound, Sampling approaches for the measurement of volatile compounds at hazardous waste sites, *J. Hazard. Mat.*, *14*, 135–148, 1987.

Bekku, Y., H. Koizumi, T. Oikawa, and H. Iwaki, Examination of four methods for measuring soil respiration, Appl. Soil Ecol., *5*, 247–254, 1997.

Corey, A. T., Air permeability, in *Methods of Soil Analysis*, 1, *Physical and Mineralogical Methods*, 2nd ed., edited by A. Klute, pp. 1121–1136, Am. Soc. of Agron., Madison, Wisc., 1986.

Czepiel, P., P. Crill, and R. Harris, Nitrous oxide emissions from municipal wastewater treatment, *Environ. Sci. Technol.*, *29*, 2352–2356, 1995.

de Mello, W. Z., and M. E. Hines, Application of static and dynamic enclosures for determining dimethyl sulfide and carbonyl sulfide exchange in *Sphagnum* peatlands: Implication for the magnitude and direction of flux, *J. Geophys. Res.*, *99*, 14,601–14,607, 1994.

de Nevers, N., *Fluid Mechanics for Chemical Engineers*, 2nd ed., McGraw-Hill, New York, 1991.

Denmead, O. T., Chamber systems for measuring nitrous oxide emission from soils in the field, *Soil Sci. Soc. Am. J.*, *43*, 89–95, 1979.

Denmead, O. T., and M. R. Raupach, Methods for measuring atmospheric gas transport in agricultural and forest systems, in *Agricultural Ecosystem Effects on Trace Gases and Global Climate Change*, *Spec. Publ. 55*, pp. 19–43, Am. Soc. of Agron., Madison, Wisc., 1993.

Gao, F., and S. R. Yates, Analysis of flux chambers for measuring VOC emissions at soil and water surface, in *Proceedings of Special Conference on Control of Emissions of Odor and Volatile Organic Compounds*, Water Environ. Fed., Alexandria, Va., 1997.

Gao, F., and S. R. Yates, Simulation of enclosure-based methods for measuring gas emissions from soil to the atmosphere, *J. Geophys. Res.*, this issue.

Gao, F., S. R. Yates, M. V. Yates, J. Gan, and F. F. Ernst, Design, fabrication, and application of a dynamic chamber for measuring gas emissions from soil, *Environ. Sci. Technol.*, *31*, 148–153, 1997.

Gholson, A. R., J. R. Ablation, R. K. M. Jayanty, J. E. Knoll, and M. R. Midgett, Evaluation of an enclosure method for measuring emissions of volatile organic compounds from quiescent liquid surface, *Environ. Sci. Technol.*, *25*, 519–524, 1991.

Jury, W. A., W. F. Spencer, and W. J. Farmer, Behavior assessment model for trace organics in soil, I, Model description, *J. Environ. Qual.*, *12*, 558–564, 1983.

Kanemasu, E. T., W. L. Powers, and J. W. Sij, Field chamber measurements of CO_2 flux from soil surface, *Soil Sci.*, *118*, 233–237, 1974.

Klute, A., and C. Dirksen, Hydraulic conductivity and diffusivity: Laboratory methods, in *Methods of Soil Analysis*, 1, *Physical and Mineralogical Methods*, 2nd ed., edited by A. Klute, pp. 687–734, Am. Soc. of Agron., Madison, Wisc., 1986.

Massmann, J. W., Applying groundwater flow models in vapor extraction system design, *J. Environ. Eng. ASCE*, *115*, 129–149, 1989.

Matthias, A. D., A. M. Blackmer, and J. M. Bremner, A simple chamber technique for field measurement of emissions of nitrous oxide from soils, *J. Environ. Qual.*, *9*, 251–256, 1980.

Moore, T. R., and N. T. Roulet, A comparison of dynamic and static chambers for methane emission measurements from subarctic fens, *Atmos. Ocean*, *29*, 102–109, 1991.

Reid, R. C., J. M. Prausnitz, and B. E. Poling, *The Properties of Gases and Liquids*, 4th ed., McGraw-Hill, New York, 1987.

Rolston, D. E., Gas flux, *Methods of Soil Analysis*, 1, *Physical and Mineralogical Methods*, 2nd ed., edited by A. Klute, pp. 1103–1119, Am. Soc. of Agron., Madison, Wisc., 1986.

Sanders, P. F., M. M. McChesney, and J. N. Seiber, Measuring pesticide volatilization from small surface areas in the field, *Bull. Environ. Contam. Toxicol.*, *35*, 569–575, 1985.

Simunek, J., and M. T. van Genuchten, The CHAIN_2D Code for simulating the two-dimensional movement of water, heat, and multiple solutes in variably-saturated porous media, *Res. Rep. 136*, 194 pp., U.S. Salinity Lab., U.S. Dep. of Agric., Riverside, Calif., 1994.

Vennard, J. K., and R. L. Street, *Elementary Fluid Mechanics*, 5th ed., John Weily, New York, 1975.

Wang, D., S. R. Yates, and J. Gan, Temperature effect on methyl bromide volatilization in soil fumigation, *J. Environ. Qual.*, *26*, 1072–1079, 1997.

Wesely, M. L., D. H. Lenschow, and O. T. Denmead, Flux measurement techniques, in *Global Troposheric Chemistry: Chemical Fluxes in the Global Atmosphere*, Natl. Cent. for Atmos. Res., Boulder, Colo., 1989.

Yagi, K., J. Williams, N.-Y. Wang, and R. J. Cicerone, Atmospheric methyl bromide (CH_3Br) from agricultural soil fumigation, *Science*, *267*, 1979–1981, 1995.

Yates, S. R., J. Gan, F. F. Ernst, and D. Wang, Methyl bromide emissions from a covered field, III, Correcting chamber flux for temperature, *J. Environ. Qual.*, *25*, 892–898, 1996.

F. Gao (corresponding author), Air Quality Management Section, Delaware Dept. of Natural Resources and Environmental Control, Dover, DE 19901. (e-mail: "fgao@dnrec.state.de.us")

S. R. Yates, Physics and Pesticide Unit, U.S. Salinity Lab., U.S. Department of Agriculture, 450 W. Big Springs Rd., Riverside, CA 92507.

(Received May 27, 1997; March 20, 1998;
accepted April 15, 1998.)